Islamic Azad University

Research Paper

Electrical Characterization of zig-zag Aluminum Thin Films Using Experimental and Theoretical Methods

Mahsa Fakharpour *,1, Maryam Gholizadeh Arashti 2, Mohammad Taghi Musazade Meybodi 3

[1] Department of Physics, Maybod Branch, Islamic Azad University, Maybod, Iran
[2] Department of Physics, Yadegar-e-Imam Khomeini (RAH) Shahre Rey Branch, Islamic Azad University, Tehran, Iran
[3] Department of Electrical Engineering, Science and Art University, Yazd, Iran

Abstract: Zig-zag Al nanostructures were fabricated on the glass and steel using thermal evaporation technique. The structural, morphology and electrical properties of Al thin films were studied by using AFM, FESEM and four-point probe instrument. FESEM analysis showed that the grains are distributed on the zig-zag Al-glass and their shape is polygonal while the grains on the zig-zag Al-steel surface have a non-uniform distribution and the shape of the grains is oval. AFM analysis indicated the surface roughness of zig-zag Al-steel nanostructures is more than the zig-zag Al-glass. Moreover, the wrinkles on the zig-zag Al-steel and the small protuberances on the zig-zag Al-glass observed. The anisotropy of electrical was performed in two perpendicular directions x and y of the samples surface. The average electrical resistivity of the zig-zag Al films on glass and steel produced were obtained about 4.69×10^{-8} and 5.85×10^{-8} Ω.m, respectively. Simulation results by the perturbation method agree with the experimental results.

*Corresponding author: Mahsa Fakharpour
Address: Department of Physics, Maybod Branch, Islamic Azad University, Maybod, Iran.   **Tell:** 00989133581318   **Email:** mahsa.fakharpour@maybodiau.ac.ir

1. INTRODUCTION

Metal structures are electrically divided into three categories: 1- Bulk metal structures that have high conductivity. 2- Homogeneous thin film structures whose conductivity depends on the thickness of the thin film and the medium homogeneity due to the reduction of cross-sectional area. The resistivity of metal thin films decreases and the conductivity increases with increasing thickness and medium homogeneity due to approaching the bulk state. 3- Nano-sculptured structures that due to the porosity of the structure, have different behaviors compared to bulk and thin film structures. The electrical properties of these nanostructures depend on various factors such as the deposition method and the geometry of the structure. Electrons in their path collide with the pores and voids of the structure, causing the electrons to scatter, resulting in increased electrical resistivity [1].

Oblique angle deposition (OAD) of thin films as method of physical vapor deposition has provided facilities for the production of variety nanostructures with structural anisotropy [1]. The electrical properties of these films have been studied by many researchers [2-5]. Various columns and shapes of nano-sculptured thin films can greatly affect their electrical properties. There are two point in determining the electrical properties of these films. The first point is that increasing the vapor incident angle increases the resistivity, which is due to the increase in porosity and voids in the film and thus the density of the film decreases. Hence, the conductivity decreases due to the voids in the film (decrease in the number of available electrical paths) [4, 5]. Second, sculptured thin film columnar microstructures do not have electrical symmetry, so the electrical resistivity varies in parallel and perpendicular directions to the nano-columns. Because the average mass density is different in different directions. Therefore, mass anisotropy causes anisotropy in the properties of the layer, including its electrical properties, so that this anisotropy increases with the vapor incident angle [5-7]. Sculptured nano-structures fabricated by this technique have wide applications such as sensors [8, 9], optical filters [10, 11], polarizers [12, 13], reflectors [14] and microchannels [15]. The Al thin films on none-metalic substrates have played an important role in modern microelectronics, i.e., integrated circuits (IC) and optical, while films formed on glass had protection and electronic.

In this work zig-zag aluminium nanostructures on glass and steel (zig-zag Al-g and zig-zag Al-s) were generated using OAD. The electrical resistivity of the thin films was obtained by measuring voltage and current using a four-point probe. The relative electrical resistivity of thin film with zig-zag geometry is

also discussed using perturbation theory. The results may be of interest due to their direct application in the microelectronics industry.

2. THEORY: ELECTRICAL RESISTIVITY USING PERTURBATION TECHNIQUE

Hori et al. [16] reported a perturbation method for calculating the electric field of two- or three-dimensional inhomogeneous medium. The relationship between current density, electric field and conductivity in electromagnetism is defined as follows [17]:

$$J_i(r) = \sigma(r) E_i(r) \tag{1}$$

$\sigma(r)$ is divided into fixed and variable parts: dependent the conductivity of the homogeneous material (σ_0) and local perturbation in the conductivity consists of voids ($\delta\sigma(r)$) [16].

$$\sigma(r) = \sigma_0 + \delta\sigma(r) \tag{2}$$

Using the electrostatic potential $\Phi(r)$ and the continuity relationship, we have [16]:

$$\Phi(r_1) = \Phi_0(r_1) + \int dr_2 g(r_{12}) \frac{\partial}{\partial x_{2,i}} \left(\delta\sigma(r_2) \frac{\partial \Phi(r_2)}{\partial x_{2,i}} \right) \tag{3}$$

Where $r_{12} = r_2 - r_1$ and the surface or volumetric integral is taken. $\Phi_0(r)$ is determined by the σ_0 and boundary conditions. The local electric field is obtained by the following equation [16]:

$$E_i(r_1) = E_i^0(r_1) + \int dr_2 G_{ij}(r_{12}) \delta\sigma(r_2) E_j(r_2) \tag{4}$$

The $E_i^0(r_1)$ is the electric field of material with σ_0 conductivity at position r_1 in a homogeneous medium. The ith component of electric field at location r_1 is $E_i(r_1)$. The Green function $G_{ij}(r_{12})$ is calculated as [16]:

$$G_{ij}(r_{12}) = -\frac{\partial^2 g(r_{12})}{\partial x_{1,i} \partial x_{2,j}} =$$

$$\begin{cases} -\dfrac{\delta_{ij}\delta(r_{12})}{3\sigma_0} + \rho\dfrac{1}{4\pi\sigma_0 r_{12}^3}\left(3\dfrac{x_{12,i}}{r_{12}}\dfrac{x_{12,j}}{r_{12}} - \delta_{ij}\right) & 3D \\[2em] -\dfrac{\delta_{ij}\delta(r_{12})}{2\sigma_0} + \rho\dfrac{1}{2\pi\sigma_0 r_{12}^2}\left(2\dfrac{x_{12,i}}{r_{12}}\dfrac{x_{12,j}}{r_{12}} - \delta_{ij}\right) & 2D \end{cases} \qquad (5)$$

Equations (4) are used to calculate the field. The thin film is considered to be a large rectangular cube. Then we divide it into very small cubes (Fig. 2 in (18)). According to the geometry of the structure, some of these small cubes on the structure have σ_0 conductivity. The remaining cubes are the same voids that has disturbed the thin film and their conductivity is chosen to be zero. With these assumptions and the conversion of integral (4) to discrete relation, equation (6) is obtained [16]:

$$E_i^0(r_k) = E_i(r_k)\left(1 + \frac{\delta\sigma(r_k)}{3\sigma_0}\right) - \sum_{j=1}^{3}\sum_{l \neq k} v_l \frac{1}{4\pi\sigma_0 r_{kl}^3}\left(3\frac{x_{kl,i}}{r_{kl}}\frac{x_{kl,j}}{r_{kl}} - \delta_{ij}\right)\delta\sigma(r_l)E_j(r_l), \qquad (6)$$

Where v_l and r_{kl} are the volume of each small cube and the distance between the two cubes kth and lth, respectively. The $x_{kl,i}$ is the ith component of r_{kl} vector.

To do the calculations, the whole layer is divided into N cubes. 3N equation is created to calculate electric fields. After solving 3N equations with 3N unknowns, the electric field is obtained. The current density of each cube is calculated by multiplying the conductivity of each cube with its electric field. The total current density is obtained by summing the current density of the cubes. As a result, electrical resistivity is provided by multiplying the total current density at the cross-section area of the layer. This resistivity is the relative resistivity of the layer (i.e., the ration of the resistivity of the porous film to a homogeneous film from the same material). Therefore, the shape of the structure is important in the perturbation theory and the substance type has nothing to do with it.

3. MATERIALS AND METHODS

Zig-zag Al nanostructures were created on the glass with size of 2 cm×1 cm as a non-conducting substrate, and on the steel with size of 2 cm×1 cm as a metal substrate by thermal evaporation technique in a Hind-HIVAC coating unit

(Model ISF6). The deposition process was repeated two times each time with five samples to confirm the results. The first, all substrates were cleaned by water soluble soap and deionized water, then the substrates were ultrasonically cleaned before loading into the chamber with acetone and ethanol for 15 min separately to thoroughly remove grease and organic contamination. Finally, the substrates were dried by purified nitrogen gas. The substrate holder was fixed obliquely in the vacuum chamber. The angle of incidence flux α with respect to the line perpendicular to the substrate was considered.

Al granol with purity of 99.99% prepared from Sigma−Aldrich Company and was evaporated from a molybdenum boat at vacuum pressure approximately of 2×10^{-7} torr. The optimal distance between the Al evaporation source and the substrate was chosen 30 cm to create a uniform film on the substrate. In order to fabrication the zig-zag Al nanostructure, the first arm was created at $\alpha=60°$ and was called zig. Then the substrate was rotated by 180° about its normal axis (angle φ) for produce the other arm (zag). The study of other properties of nanostructures has been reported in our previous research [18, 19]. In order to better identify the samples, the following codes have been assigned to them. The samples of zig-zag Al on glass and steel are named as zigzag Al-g and zigzag Al-s.

Film thickness and structure morphology were obtained using FESEM (Hitachi S-4100 SEM). The surface of the thin films was covered with a thin layer of gold to prevent the charging effect. The average and root square surface roughness of the samples were obtained by AFM (NT-MDT, SOLVER, Nova Tech) analysis with a Si tip of 10 nm in diameter and in non-contact mode. In order to characterization the electrical properties of samples, all deposited samples were tested by four-point probe method.

4. RESULTS AND DISCUSSION

A. *Structure and surface morphology of zig-zag Al nanostructures*

Fig. 1(a-b) shows the FESEM images of the zig-zag Al nanostructures on the glass and steel, respectively. Also, the typical cross-sectional view FESEM images of the zig-zag Al nanostructures with two arms on the glass is shown in Fig. 1(c) by FESEM.

From Fig. 1(a) and (b) obvious that the grains formed on zig-zag Al-g surface are evenly distributed and their shape is polygonal while the grains formed on the zig-zag Al-s surface have a non-uniform distribution and the shape of the grains is oval. Also, because of warming the substrate surface during the

deposition, the grains size on the zig-zag Al-g sample is larger than the zig-zag Al-s sample. According to the cross-sectional FESEM images (Fig. 1(c)), the layer thickness was 500±10 nm. In addition to the uneven distribution of grains, the ups and downs created on the surface increase the roughness of the film surface. The type of substrate affects the structural properties of the thin film [20]. Khachatryan et al. [21] showed that grain growth on steel takes place in several stages. In the first stage, islands are formed and then they grow to form seeds. In the second stage, the secondary nucleation is filled the depressions to form a continuous film. Unlike steel, the grain growth on glass takes place in a single stage to the islands develop into a continuous film. It was found that these differences in microstructure affected the film's electrical properties.

The compressed nanorods in the lower layers can be seen in the cross-sectional FESEM image of the zig-zag Al-g sample (Fig. 1(c)). In addition, the arms diameter increases with increasing thickness. The growth angle and arms length obtained from the FESEM image are 60° and 250 nm, respectively.
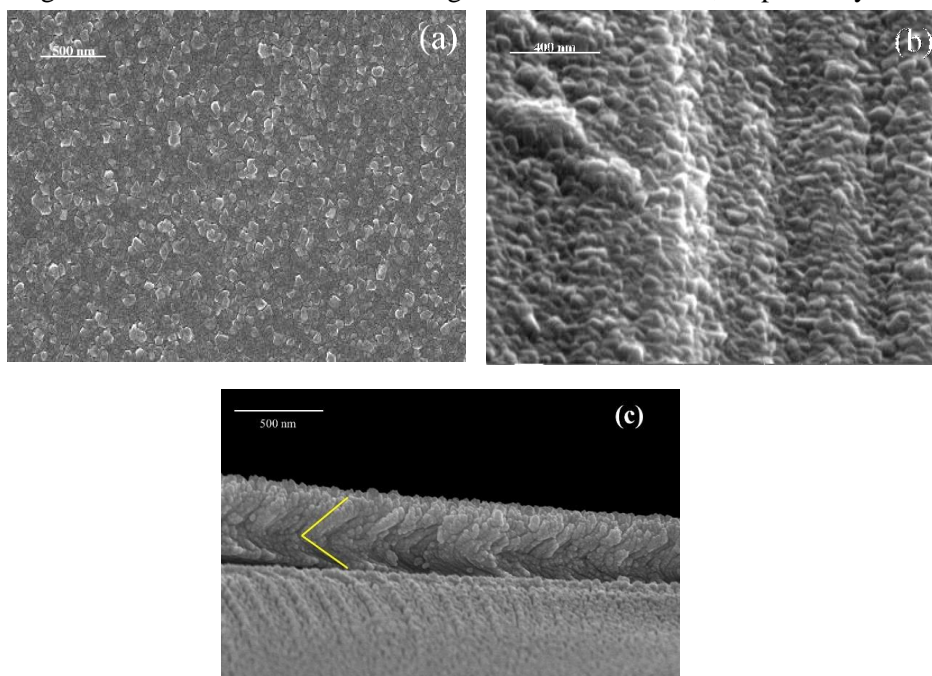

Fig. 1. Top view FESEM micrographs of zig-zag Al nanostructures with 2 arms on (a) glass, (b) steel, and (c) cross-section view FESEM micrograph of zig-zag Al nanostructure with 2 arms on glass

Fig. 2, shows the two-dimensional and three-dimensional AFM images (columns I and II) of zig-zag Al nanostructure produced on the glass and steel (Rows (a) and (b)). The grain size, average (Rave) and root mean square (Rrms) surface roughness of samples obtained from the AFM results by Nanoscope software and are given in Table 1.
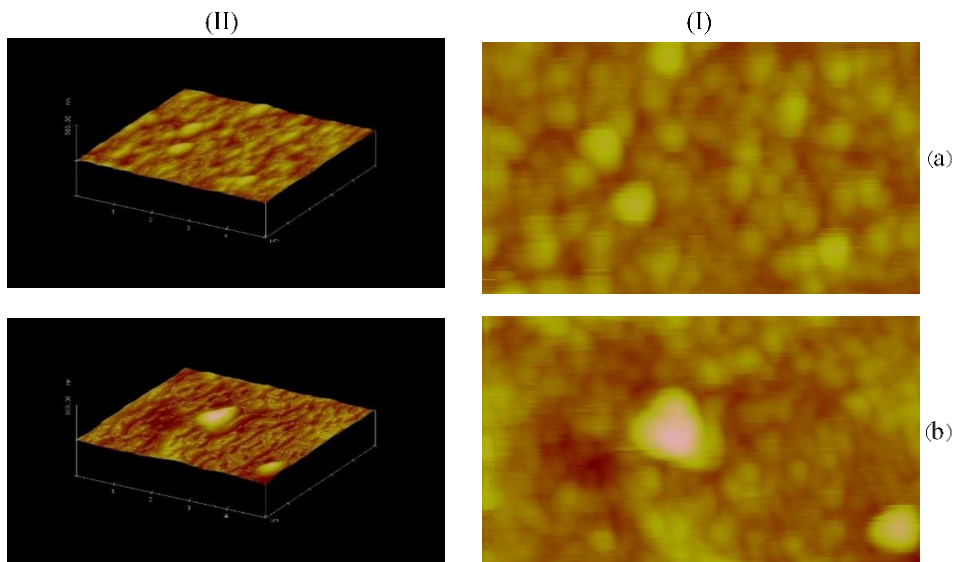

Fig. 2. 5 μm × 5 μm AFM topography of zig-zag Al nanostrucrures on the different substrates; column (I) two-dimensional images; column (II) three-dimensional images. Row (a) glass substrate; Row (b) steel substrate.

The surface roughness of the zig-zag Al-s sample is greater than that of the zig-zag Al-g sample as shown in Table 1. The three-dimensional AFM images of the zigzag Al-s (column II, row (b)) and Al-g samples (column II, row (a)) show the wrinkles and the small bumps on the surface, respectively. This may be due to the lower amount of surface roughness of the glass. On the other hand, the nanostructure formed on steel is non-uniform, while the nanostructure on glass is uniform. These results prove that the growth process on steel and glass is different.

TABLE I
DIFFERENT CHARACTERISTICS OF ZIG-ZAG AL NANOSTRUCTURES ON GLASS AND STEEL

Sample	d (nm)	D_{AFM} (nm)	R_{rms} (nm)	R_{ave} (nm)	$\rho_x \times 10^{-8}$ (Ω.m)	$\rho_y \times 10^{-8}$ (Ω.m)	$\rho_{ave} \times 10^{-8}$ (Ω.m)	R_s (Ω)	A
ZigzagAl-g	500	167.70	5.310	4.027	4.90±0.81	4.47±1.72	4.69	9.38	0.04
ZigzagAl-s	500	128.04	8.238	5.488	6.40±2.77	5.31±1.91	5.85	11.7	0.09

D_{AFM} is grain size obtained from AFM analysis; R_{ave} and R_{rms} are average and root square surface roughness; ρ_x, ρ_y, and ρ_{ave} are average electrical resistivity and electrical resistivity at directions of x and y, respectively; R_s and A are sheet resistance and anisotropy.

B. Electrical resistivity

Aluminum reacts very quickly with oxygen, so after deposition it must be stored in special containers and electrical measurements performed quickly. The I-V curves were obtained using a four-point probe tool and then the electrical resistivity of the zig-zag Al films was calculated from the diagrams. Measurements were performed in two perpendicular directions x and y of the sample surface as shown in Fig. 3. These measurements give us the data needed to determine the degree of anisotropy in the nanostructure of the samples produced in this work on different substrates. Resistivity of the films was calculated using [22, 23]:

$$\rho = \frac{\pi d}{\ln 2}(\frac{V}{I})$$

$$\rho \approx 4.532d\,(\frac{V}{I}) \tag{7}$$

Where *V, I,* and *d* are the drop potential measured among the internal electrodes in mV, the current in mA and thickness of thin film, respectively. The electrical conductivity of the films can be obtained by $\sigma = \frac{1}{\rho}$.
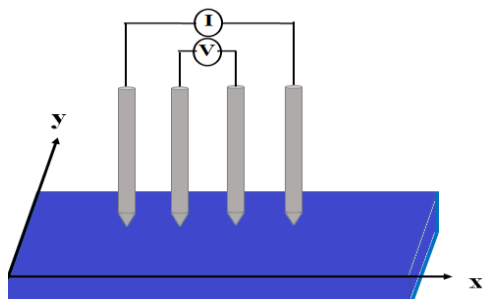
Fig. 3. Schematic diagram of the four-point probe used for the measurement of electrical resistivity of zig-zag Al thin films.

By knowing the values of ρ and the thickness of the thin films, the sheet resistivity can be determined according to the equation (4) [22, 23]:

$$R_s = \frac{\rho}{d} \tag{8}$$

The uncertainty of these results was obtained as [24]:

$$\Delta\rho = \frac{\pi d}{\ln 2}\left(\frac{v}{I}\right)\sqrt{\left(\frac{\Delta v}{v}\right)^2 + \left(\frac{\Delta I}{I}\right)^2}. \tag{9}$$

As mentioned before due to anisotropic structure of these films their anisotropy was achieved using:

$$Anisotropy = \frac{\rho_x - \rho_y}{\rho_x + \rho_y}. \tag{10}$$

Fig. 4 shows the I-V curves of the zig-zag Al nanostructures on glass and steel substrates in two different directions x and y. The electrical resistivity in both directions (ρ_x and ρ_y) is obtained from (7), and by averaging them, the average resistivity ρ_{ave} of each sample is calculated. Factors that can change the resistivity of the structures produced in this work include surface roughness, structure geometry, substrate, and grain sizes.
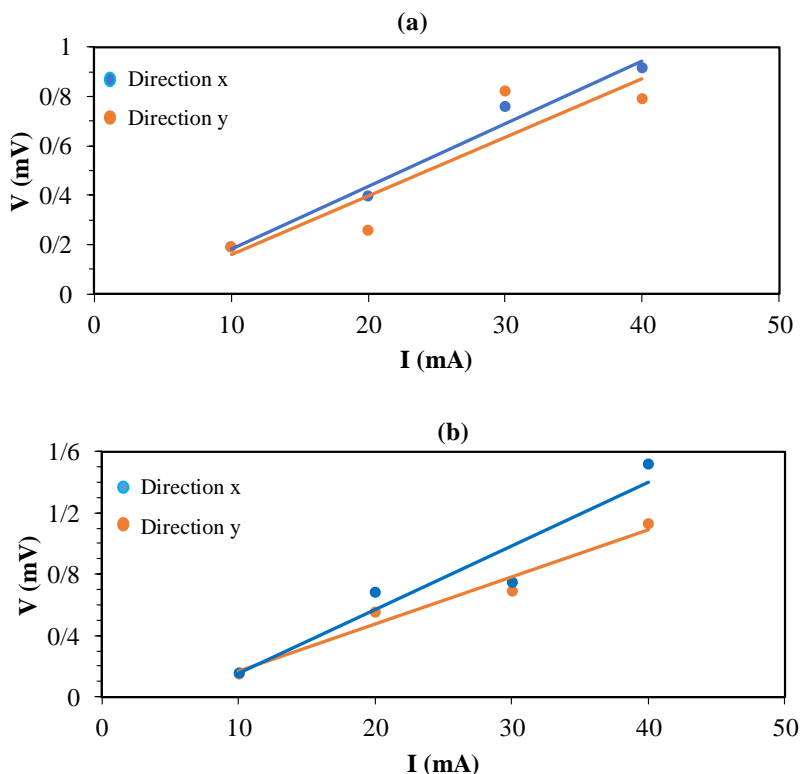
(a)

(b)

Fig. 4. I-V curves for zig-zag Al structures on a) glass and b) steel

The results are described in the following paragraphs:

a) Since the slope of the I-V curves (Fig. 4) is different for the x and y directions, the prepared nanostructures have heterogeneous and anisotropic electrical properties on the surface. As a result, the resistivity of the samples is not the same in different directions. Since the slope of the I-V curves (Fig. 4) is different for the x and y directions, the prepared nanostructures have heterogeneous and anisotropic electrical properties on the surface.

b) The slope of I-V curves (Fig. 4) in the x direction for both samples of zig-zag Al-g and zig-zag Al-s is higher than the y direction. Oblique deposition and zig-zag morphology of the nanostructure are the cause of anisotropy and change in the slope of the curves in different directions x and y.

c) The electrical resistivity of zig-zag Al-g and zig-zag Al-s samples is higher than the bulk value of 2.42×10^{-8} Ω.m [25], as given in Table 1. Qui et. al [26] have also reported the resistivity of aluminum films deposited on glass

substrates for thicknesses of 448 nm and 658 nm at deposition rate of 33 nm/min about 3.3×10^{-8} and 4.2×10^{-8} Ω.m, respectively. Panta et.al [27] were fabricated Al thin films with different thickness by PVD technique on glass substrates. The electrical resistivity of films varied from 3.1×10^{-8} to 8.3×10^{-8} Ω.m with thickness ranging from 148 nm to 225 nm, respectively. The average electrical resistivity of the zig-zag Al-g and zig-zag Al-s films produced in this work were obtained about 4.69×10^{-8} and 5.85×10^{-8} Ω.m, respectively, as shown in Table. 1. Boundary grains and porosity affect the electrical resistivity of samples. Electrons collide with these pores, grain boundaries, other defects, and impurities as they pass through the path and scatter. As a result, the conductivity of the samples is decreased with increasing voids.

d) The electrical resistivity of zig-zag Al-s sample is higher than zig-zag Al-g, depending on the surface roughness and grain size. The resistivity is increased with increasing the surface roughness, hence more electron scattering from surface roughness may occur which in turn increases the resistivity of the sample. As can be seen from Table 1, the surface roughness of zig-zag Al-s sample is higher than zig-zag Al-g, so the resistivity or slope of the V-I curve of zig-zag Al-s sample is greater than that of zig-zag Al-g.

Another important point is the effect of grain size on resistivity. The electron scattering in the grain boundaries depends on the grain size and decreasing the electron scattering or increasing the average free path reduces the resistivity and increases the conductivity. According to Table 1, the grain size of the zig-zag Al-g sample is larger than the zig-zag Al-s sample, so the electrical resistance of zig-zag Al-g is less than that of zig-zag Al-s. Barna et. al [28], Reicha et. al [29] also showed that films with small grain sizes have weaker electrical properties.

e) In Table. 1 results of the anisotropy of the samples obtained from equation (9) are given. The degree of electrical anisotropy of the zig-zag Al-g sample is lower than that of zig-zag Al-s. This could be due to the uniform surface on the zig-zag Al-g sample surface. In the zig-zag Al-s sample, the protuberances are parallel and in one direction, so the electrical resistivity is more different in the two directions and the anisotropy has a higher degree.

C. *Estimating the resistivity of zig-zag thin film*

In perturbation method, the structure is considered as a two- or three phase composites of metal-nonmetal inhomogeneous medium. In this model, the electrical resistance of heterogeneous thin films to homogeneous thin films is calculated in terms of the morphology of the structure and the volume fraction

of the material. In this study, zig-zag Al thin film is considered as a composite with two different phases including porosity phase and aluminum phase in a heterogeneous environment, which depends on the column shape factor and the porosity fraction phase, and we calculate to the resistance of our samples as relative resistance. As explained in the theory section, to calculate the relative resistivity, the zig-zag thin film was selected as a rectangular cube with a × b × h dimensions. This cube was then divided into many small cubes of length d so that they are equidistant from each other. It should be noted that the dimensions of a rectangular cube are a multiple of the size of the side of a small cube length d so that calculations can be performed with dimensionless lengths. Then the geometry of the structure is chosen, some small cubes are selected from inside the rectangular cube to make the zig-zag structure with σ_0 conductivity. The remaining cubes are the same porosities and their conductivity is assumed to be zero. The structure of zig-zag Al prepared in the deposition has the same lengths. Hence, in the perturbation simulation, the length of the zig and zag arms was assumed 3d. Therefore, a cube is chosen with 3d × 3d × h dimensions. Where h (cubic height) is the thickness of the film. The relative resistivity obtained by this method does not depend on the dimensions of the nanostructure and the type of substrate and only depend on the geometry of the structure and the voids. In order to perform simulation work on the electrical resistance of the Al thin film samples, as discussed in the preceding section in this calculation, for each value of material inclusion, 3d × 3d × h cubes are involved and a system of 3 × 3d × 3d × h equations with the same number of unknowns is solved. After solving 3N equations with 3N unknowns, the electric field is obtained. The local current density is calculated using equation (1). The electric current of each cube is obtained by multiplying the current density component of each cube in a certain direction by the cross-sectional area of the same cube. Then, from the sum of the currents, the total electric current is obtained. Having the total current, the electrical resistance can be calculated. Fig. 5 shows the results of relative resistivity (zig-zag structure resistivity relative to a homogeneous structure with the same dimensions) as a function of material fraction for zig-zag Al nanostructures using equations (1) to (6) and the simulated work. It can be observed that in the zig-zag structures the resistivity increases by decreasing material inclusion. This is consistent with Siabi-Garjan et al.s' results [30] for columnar structures and Fakharpour et al.s' results [31] for graded helical square tower-like nanostructures. Therefore, simulation using perturbation method can show the effect of structure morphology on electrical resistance.
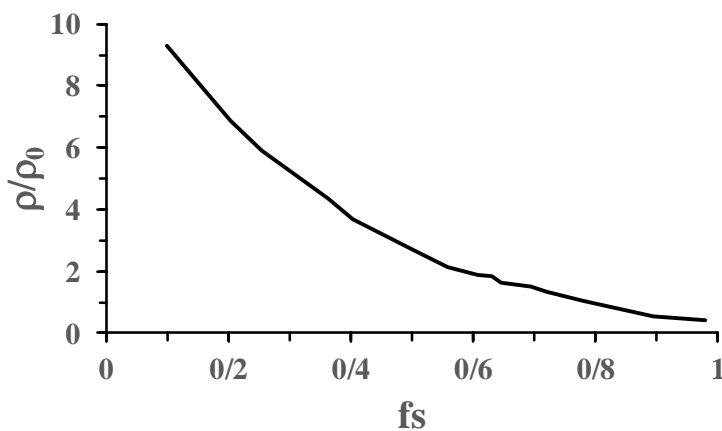
Fig. 5. Relative resistivity of zig-zag Al structures as a function of material fraction.

4. CONCLUSION

Zig-zag Al nanostructures were fabricated on the glass and steel by thermal evaporation technique. The anisotropy of electrical was performed in two perpendicular directions x and y of the sample surface. The electrical resistivity in the x direction for both samples of zig-zag Al-g and zig-zag Al-s is higher than the y direction. Average electrical resistivity of zig-zag Al-s sample is higher than zig-zag Al-g. Also, the degree of electrical anisotropy of the zig-zag Al-g sample is lower than that of zig-zag Al-s. This could be due to the uniform surface on the zig-zag Al-g sample surface. The results of the simulated model using perturbation theory are consistent with the experimental results.

CONFLICT OF INTEREST

The authors declare that there is no conflict of interests regarding the publication of this manuscript.

REFERENCES

[1] M. M. Hawkeye, M. J. Brett. *Glancing angle deposition: fabrication, properties, and applications of micro-and nanostructured thin films*. Journal of Vacuum Science & Technology A: Vacuum, Surfaces, and Films. 25(5) (2007, Sep) 1317-1335. Available: https://doi.org/10.1116/1.2764082.

[2] R. Yahyazadeh, Z. Hashempour, *Numerical Modeling of Electronic and Electrical Characteristics of 0.3 0.7 Al Ga N/GaN Multiple Quantum Well Solar Cells*. Journal of Optoelectronical Nanostructures. 5(3) (2020, Sep) 81-102. Available: 20.1001.1.24237361.2020.5.3.6.5.

[3] S. Rafiee Rafat, Z. Ahangari, M. M. Ahadian. *Performance Investigation of a Perovskite Solar Cell with TiO2 and One Dimensional ZnO Nanorods as Electron Transport Layers*. Journal of Optoelectronical Nanostructures. 6(2) (2021, Jun) 75-90. Available: https://doi:10.30495/JOPN.2021.28208.1224.

[4] J. Lintymer, J. Gavoille, N. Martin, J. Takadoum. *Glancing angle deposition to modify microstructure and properties of sputter deposited chromium thin films*. Surface and Coatings Technology. 174(1) (2003, Sep) 316-323. Available: https://doi.org/10.1016/S0257-8972(03)00413-4.

[5] D. Vick, M. Brett. *Conduction anisotropy in porous thin films with chevron microstructures*. Journal of Vacuum Science & Technology A: Vacuum, Surfaces, and Films. 24(1) (2006, Jan) 156-164. Available: https://doi:10.1116/1.2148413.

[6] K. Kuwahara, S. Shinzato. *Resistivity anisotropy of nickel films induced by oblique incidence sputter deposition*. Thin Solid Films. 164(1) (1988, Oct) 165-168. Available: https://doi.org/10.1016/0040-6090(88)90128-9

[7] K. Okamoto, K. Itoh. *Incidence angle dependences of columnar grain structure and texture in obliquely deposited iron films*. Japanese journal of applied physics. 44(3R) (2005, Mar) 1382. Available: https://doi.org/10.1143/JJAP.44.1382.

[8] M. A. Badshah, D. Michel, N.E. Alam, I. Madni, N. Abbas, K. Alameh, Seok min Kim. *Enhancing the Sensitivity of a Surface Plasmon Resonance Sensor with Glancing Angle Deposited Nanostructures*. Plasmonics. 15(6) (2020, Dec) 2161-2168. Available: https://doi.org/10.1007/s11468-020-01245-0.

[9] A. Moftakharzadeh, B. Afkhami Aghda, M. Hosseini. *Noise Equivalent Power Optimization of Graphene-Superconductor Optical Sensors in the*

Current Bias Mode. Journal of Optoelectronical Nanostructures. 3(3) (2018, Sep) 1-12. Available: 20.1001.1.24237361.2018.3.3.1.6.

[10] V. Fallahi, M. Seifouri. *Novel structure of optical add/drop filters and multi-channel filter based on photonic crystal for using in optical telecommunication devices.* Journal of Optoelectronical Nanostructures. 4(2) (2019, Jun) 53-68. Available: 20.1001.1.24237361.2019.4.2.5.5.

[11] M. Gholizadeh, R. Z. Moghadam, A. Mohammadi, M. Ehsani, H. R. Dizaji. *Design and fabrication of MgF2 sinle-layer antireflection coating by glancing angle deposition.* Materials Research Innovations. 24(7) (2020, Nov) 442-446. Available: https://doi.org/10.1080/14328917.2020.1723991.

[12] A. Ruder, B. Wright, D. Peev, R. Feder, U. Kilic, M. Hilfiker. *Mueller matrix ellipsometer using dual continuously rotating anisotropic mirrors.* Optics Letters. 45(13) (2020, Jul) 3541-3544. Available: https://doi.org/10.1364/OL.398060.

[13] T. Tolenis, L. Grineviciute, A. Melninkaitis, R. Buzelis. *High Reflectivity Coatings based on Sculptured Thin Films.* Optical Interference Coatings; (2019, Jun) MD-3. Available: https://doi.org/10.1364/OIC.2019.MD.3.

[14] S. Bairagi, K. Järrendahl, F. Eriksson, L. Hultman, J. Birch, C. L. Hsiao. *Glancing Angle Deposition and Growth Mechanism of Inclined AlN Nanostructures Using Reactive Magnetron Sputtering.* Coatings. 10(8) (2020, Aug) 768. Available: https://doi.org/10.3390/coatings10080768.

[15] K. W. Jung. *Investigating Thermo-Fluidic Performance of Si-Based Embedded Microchannels-3D Manifold Cooling System for High Power Density Electronic Applications,* Stanford University, ProQuest Dissertations Publishing, 2020. 28104043. Available: https://stacks.stanford.edu/file/druid:zb171kw6421/PhD_Thesis-KiWookJung-final-augmented.pdf.

[16] M. Hori, F. Yonezawa. *Theoretical approaches to inhomogeneous transport in disordered media.* Journal of Physics C: Solid State Physics. 10(2) (1977, Jan) 229. Available: https://doi.org/10.1088/0022-3719/10/2/009.

[17] D, Jackson, *Classical Electrodynamiccs*, 3nd ed. New York: Wiley, 1999. https://doi.org/10.1119/1.19136.

[18] M. Gholizadeh Arashti, M. Fakharpour. *Fabrication and characterization of Al/glass zig-zag thin film, comparing to the discrete dipole approximation results.* European Physical Journal B--Condensed Matter.

93(5) (2020, May) 1-6. Available: https://doi.org/10.1140/epjb/e2020-100581-0.

[19] M. Fakharpour, G. Taheri. *Fabrication of Al zigzag thin films and evaluation of mechanical and hydrophobic properties*. Applied Physics A. 126(8) (2020, July) 1-8. Available: https://doi.org/10.1007/s00339-020-03773-2.

[20] S. Manouchehri, J. Zahmatkesh, M. H. Yousefi. *Substrate effects on the structural properties of thin films of lead sulfide*. Journal of Optoelectronical Nanostructures. 3(2) (2018, Jun) 1-18. Available: 20.1001.1.24237361.2018.3.2.1.4.

[21] H. Khachatryan, S. N. Lee, K. B. Kim, H. K. Kim, M. Kim. *Al thin film: The effect of substrate type on Al film formation and morphology*. Journal of Physics and Chemistry of Solids. 122 (2018, Nov) 109-117. Available: https://doi.org/10.1016/j.jpcs.2018.06.018.

[22] K. L. Chopra, *Thin film phenomena*, Journal of The Electrochemical Society. 117(5) (1970, May) 180Cb. Available: https://doi.org/10.1149/1.2407581.

[23] D. Campbell. *Handbook of Thin Film Technology* (LI Maissel and R. Glang, eds.), New York: McGraw-Hill Book Co,1970, p (12-1) - (12-50). Available: https://doi.org/10.1117/12.559785

[24] H. Savaloni, F. Babaei, S. Song, F. Placido. *Influence of substrate rotation speed on the nanostructure of sculptured Cu thin films.* Vacuum. 85(7) (2011, Jan) 776-781. Available: https://doi.org/10.1016/ j. vacuum.2010.11.017.

[25] G. Kaye, T. Laby, *Tables of physical and chemical constants*. Essex, England. New York: Longman; Print book, English, 16th ed, 1995. Available: https://doi.org/10.1002/jctb.5000554445.

[26] H. Qiu, F. Wang, P. Wu, L. Pan, L. Li, L. Xiong. *Effect of deposition rate on structural and electrical properties of Al films deposited on glass by electron beam evaporation.* Thin Solid Films. 414(1) (2002, Jul) 150-153. Available: https://doi.org/10.1016/S0040-6090(02)00454-6.

[27] G. P. Panta, D. P. Subedi. *Electrical characterization of aluminum (Al) thin films measured by using four-point probe method.* Kathmandu University journal of science, Engineering and technology. 8(2) (2012, Dec) 31-36. Available: https://doi.org/10.3126/KUSET.V8I2.7322.

[28] A. Barna, P. Barna, G. Radnoczi, F. Reicha, L. Toth. *Formation of aluminium thin films in the presence of oxygen and nickel.* Physica status solidi (a). 55(2) (1979, Oct) 427-435. Available: https://doi.org/10.1002/pssa.2210550210.

[29] F. Reicha, M. El. Hiti, P. Barna. *Electrical properties of thin oxidized aluminium films.* Journal of materials science. 26(8) (1991, Apr) 2007-2014. Available: https://doi.org/10.1007/BF00549159.

[30] A. Siabi-Garjan, H. Savaloni. *Extinction spectra and electric near-field distribution of Mn nano-rod based sculptured thin films: experimental and discrete dipole approximation results.* Plasmonics. 10(4)) 2015, Aug) 861-872. Available: https://doi.org/10.1007/s11468-014-9873-2.

[31] M. Fakharpour, H. Savaloni. *Fabrication of graded helical square tower-like Mn sculptured thin films and investigation of their electrical properties: comparison with perturbation theory.* Journal of Theoretical and Applied Physics. 11(2) (2017, Jun) 109-117. Available: https://doi.org/10.1007/s40094-017-0242-3.